Macroscale Superlubricity and Polymorphism of Long-Chain *n*-Alcohols

Tom Reddyhoff,[1,*] James P. Ewen,[1,*] Pushkar Deshpande,[1] Mark D. Frogley,[2] Mark D. Welch,[3] and Wren Montgomery[4,5]

[1] Department of Mechanical Engineering, Imperial College London, Exhibition Road, South Kensington, London, SW7 2AZ, United Kingdom.

[2] Soft Condensed Matter Group, Diamond Light Source, Diamond House, Harwell Science and Innovation Campus, OX11 0DE Didcot, United Kingdom.

[3] Department of Earth Sciences, The Natural History Museum, Cromwell Road, South Kensington, London, SW7 5BD, United Kingdom.

[4] Department of Earth Science and Engineering, Imperial College London, Exhibition Road, South Kensington, London, SW7 2AZ, United Kingdom.

[5] Imaging and Analysis Centre, The Natural History Museum, Cromwell Road, South Kensington, London, SW7 5BD, United Kingdom.

* Corresponding author email addresses t.reddyhoff@imperial.ac.uk ; j.ewen@imperial.ac.uk

KEYWORDS

Friction, Superlubricity, Polymorphism, Elastohydrodynamic Lubrication, Tribology, 1-Dodecanol

ABSTRACT

Simple *n*-alcohols, such as 1-dodecanol, show anomalous film-forming and friction behaviour under elastohydrodynamic lubrication (EHL) conditions, as found inside bearings and gears. Using tribometer, diamond anvil cell (DAC), and differential scanning calorimetry (DSC) experiments, we show that liquid 1-dodecanol undergoes pressure-induced solidification when entrained into EHL contacts. Different solid polymorphs are formed inside the contact depending on the temperature and pressure conditions. Surprisingly, at moderate temperature and pressure, 1-dodecanol forms a polymorph that exhibits robust macroscale superlubricity. The DAC and DSC experiments show that superlubricity is facilitated by the formation of lamellar, hydrogen-bonded structures of hexagonally close-packed molecules, which promote interlayer sliding. This novel superlubricity mechanism is similar to that proposed for the two-dimensional materials commonly employed as solid lubricants, but it also enables the practical advantages of liquid lubricants to be maintained. When the pressure is increased, 1-dodecanol undergoes a polymorphic transformation into a phase that gives higher friction. The DAC and DSC experiments indicate that the high-friction polymorph is an orthorhombic crystal. The polymorphic transformation pressure coincides with the onset of dimple formation in the EHL films, revealing that the anomalous film shapes are caused by the formation of rigid orthorhombic crystals inside the contact. This is the first demonstration of macroscale superlubricity in an EHL contact lubricated by a non-aqueous liquid that arises from bulk effects rather than tribochemical transformations at the surfaces. Since the superlubricity observed here results from phase transformations, it is continuously self-replenishing and is insensitive to surface chemistry and topology. This discovery creates the possibility of implementing superlubricity in a wide range of machine components, which would result in enormous improvements in efficiency and durability.

1. INTRODUCTION

Recent estimations suggest that ~23% of the world's total energy consumption originates from tribological contacts.[1] There are currently more than 50 billion rolling bearings in operation worldwide, making them the most common lubricated engineering components.[2] Bearings, along with gears, constant velocity joints, and cam/follower systems, are based on elements that both roll and slide together. Due to the curvature of these load-bearing components, contact areas between sliding surfaces are typically only hundreds of microns in diameter, which leads to very high (≥ 1 GPa) pressures. When lubricated by viscous fluids, such as hydrocarbon base oils, these conditions give rise to elastohydrodynamic lubrication (EHL). Under EHL conditions, elastic deformation of the non-conformal surfaces, and a sharp increase in lubricant viscosity, leads to lubricant films that are thicker than would otherwise be expected.[3] These lubricant films play a critical role in machine performance and reliability since their thickness determines durability and their friction determines energy dissipation and hence efficiency.[4]

For a standard internal combustion engine (ICE)-powered passenger car, the energy loss due to EHL friction is estimated to account for ~18 % of the total fuel consumption.[5] This is a significant quantity of fuel considering that the energy efficiency of ICE-powered vehicles is generally only ~20 %.[6] Moreover, the proportion of total energy losses due to EHL friction is likely to increase with the shift from ICEs to hybrid and electric powertrains.[6] Consequently, there is an urgent need to develop lubricants that provide lower EHL friction. Recently, Zhang et al.[7] measured the EHL friction for several commercial and prototypical base oils with a wide range of chemistries and molecular structures. They found that EHL friction coefficients, μ, varied between 0.04-0.12 for high-temperature (60-100 °C), high-pressure (1.5-2.0 GPa) conditions.[7] An ideal goal to improve energy efficiency and durability would be to implement macroscale liquid superlubricity ($\mu < 0.01$[8]) inside EHL contacts.[1]

Hirano and Shinjo[9] predicted that the friction coefficient should vanish for certain configurations of contacting crystalline surfaces. They later named the behaviour 'superlubricity' and proposed the $\mu < 0.01$ threshold value.[8] Over the last decade, superlubricity has been observed in mostly nanoscale contacts lubricated with two-dimensional materials[8] such as graphite,[10] molybdenum disulphide,[11] graphene,[12] and graphene/boron nitride.[13] In these examples, structural superlubricity[9] results from interlayer sliding of lamellar surfaces that are incommensurate, either as a result of a misalignment angle[10] or heterojunctions, where there is an intrinsic lattice mismatch between adjacent layers.[13] These effects suppress stick-slip motion by eliminating the energy dissipation

channel related to elastic instabilities. Several recent studies have demonstrated that superlubricity can also be achieved in microscale contacts, as reviewed by Hod et al.[14]. In one pertinent example, Smith et al.[15] showed that *n*-dodecane displays microscale superlubricity when confined to a single molecular layer between crystallographically misaligned, atomically smooth mica surfaces in a surface force balance. Macroscale superlubricity was recently achieved by Berman et al.[16] in a silica-diamond-like-carbon (DLC) contact using a combination of graphene and nanodiamonds as a solid lubricant in a dry nitrogen environment. Over the last decade, some systems have also been identified that can provide macroscale superlubricity in liquid-lubricated contacts.[17] The majority of these systems are aqueous-based and most also require tribochemical transformations of the surfaces during a running-in period before they achieve superlubricity.[17] Kano an co-workers[18] showed that DLC surfaces can provide macroscale superlubricity under boundary lubrication conditions using glycerol mono-oleate dissolved in a hydrocarbon base oil. Similar behaviour was also noted for pure polyhydric alcohols.[19] However, none of these systems have yielded superlubricity under full-film EHL conditions relevant for bearings, gears, and many other automotive components.

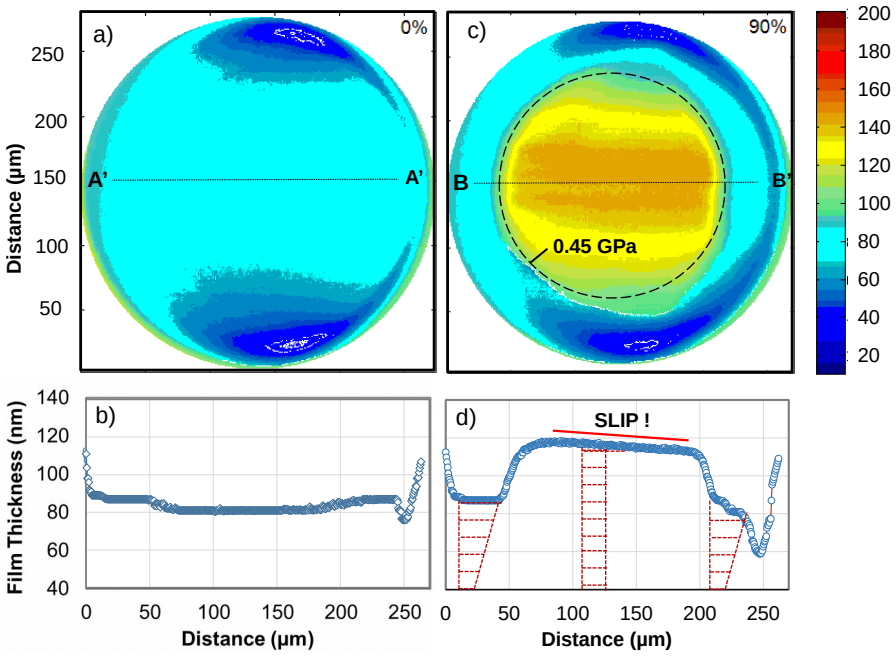

Figure 1. (a) Film thickness distribution for an EHL contact lubricated by 1-dodecanol with pure rolling (SRR = 0 %), entrainment speed = 1 m s^{-1}, load = 20 N, temperature = 40 °C. (b) Film thickness profile along the centre of the contact (section A-A') with pure rolling. (c) Anomalous EHL film thickness distribution (dimple formation) at high SRR. (d) Film thickness profile along the centre of the contact (section B-B') with SRR = 90 %. Red arrows in (d) indicate that Couette flow occurs in the inlet and outlet, while slip occurs in the centre of the contact, due to solidification.[20] Adapted from Wang and Reddyhoff.[21]

Figure 1a shows a typical film thickness distribution inside an EHL contact, produced in this case between a ball and a transparent disk, measured using ultrathin-film interferometry.[21] The lubricant enters the contact on the left and the viscosity increases by several orders of magnitude due to the steep pressure gradient. At such high viscosities, only a very shallow gradient is needed to generate sufficient hydrodynamic pressure to balance the applied load, so the film thickness in the central region is approximately constant (see Figure 1b). Furthermore, due to negligible side leakage, the value of film thickness in this central region depends only upon the fluid viscosity in the inlet zone, where pressures are relatively low (100 MPa).[4] As the lubricant subsequently exits the contact, the steep negative pressure gradient, and the consequent reduction in viscosity, hasten the flow of lubricant outward. To maintain the continuity of flow, the film thickness reduces locally and produces a horseshoe-shaped constriction (Figure 1a).[22]

The ratio of the sliding speed to the entrainment speed, the slide-roll-ratio (SRR), is used as a proxy measure for the shear rate inside EHL contacts. Recent research has suggested that *n*-alcohols, such as 1-dodecanol, exhibit unusual film-forming behaviour under EHL conditions at high SRR. Yagi and Vergne[23] showed that while 1-dodecanol behaves normally under pure rolling conditions (Figure 1a-b), a large central dimple forms at high SRR (Figure 1c-d). The authors concluded that neither the thermal wedge effect (caused by frictional heating[24]) nor the viscosity wedge effect (resulting from a temperature gradient across the fluid film[25]) could explain the anomalous film shapes, since the temperature increase of the lubricant was always less than 25 °C. Dimple formation was first observed in EHL experiments by Kaneta et al.[26] for a range of base oils with much higher viscosity than 1-dodecanol. Using numerical methods, Ehret et al.[20] explained dimple formation by assuming solidification in the central high-pressure region of the contact. More recently, Wang and Reddyhoff[21] showed that the anomalous film-forming behaviour of 1-dodecanol could be explained by assuming that slip occurs close to the solid-liquid interfaces. At low SRR, the central fluid film thicknesses measured by Wang and Reddyhoff[21] were consistent with predictions using the Hamrock-Dowson equation,[27] but they were much thicker than predicted at high SRR.[21]

In another study, Yagi and Vergne[28] compared the EHL film-forming behaviour of 1-dodecanol to 1-decanol and 1-tetradecanol. They found that the film thickening in the centre of the contact under high SRR conditions was smallest for 1-decanol (lowest melting point) and largest for 1-tetradecanol (highest melting point). Yagi et al.[29] compared the EHL film

formation and friction for a wider range of alcohols and related molecules. They found that linear mono-alcohols, -carboxylic acids, -amines, and -chlorides produced anomalous film shapes and friction behaviour, while diols, triols, and phenols produced conventional EHL film shapes and friction behaviour. More specifically, the friction coefficient of the *n*-alcohols, carboxylic acids, amines, and chlorides increased sharply at low SRR and then decreased to very low values (μ < 0.01) at high SRR.[29] On the other hand, diols, triols, and phenols showed a gradual increase in friction coefficient with SRR,[29] as is typically observed for lubricant base oils.[7]

In the liquid phase, competing hydrophilic and hydrophobic interactions cause short-chain *n*-alcohols (*e.g.* methanol, ethanol) to form ring-like hydrogen-bonded clusters,[30] while long-chain *n*-alcohols (*e.g.* 1-octanol, 1-decanol) generally form chain-like clusters.[31] The extent of *n*-alcohol hydrogen bonding decreases upon an increase in temperature.[32] Some studies have suggested that hydrogen bonding strength in *n*-alcohols also decreases with increasing pressure,[32] although more recent studies have shown the opposite trend.[33]

Tribology studies have suggested that solidification plays a central role to the unusual film formation and friction behaviour of *n*-alcohols under EHL conditions.[21,23,28,29] Upon solidification, long-chain *n*-alcohols are known to display polymorphism.[34] 1-dodecanol has a melting point of 24 °C at atmospheric pressure.[35] When it is cooled below this temperature, 1-dodecanol mostly forms an orthorhombic β-phase, where the hydrocarbon chains are vertical to the plane of the end groups.[35] Other *n*-alcohol polymorphs include a hexagonal α-phase, where the hydrocarbon chains are vertical to the plane of the end groups. The α-phase is usually only metastable and exists in a narrow temperature range at atmospheric pressure.[36] The α-phase has a larger volume than the other phases,[35] and it is sometimes interpreted as a rotator phase,[34] similar to those previously identified in *n*-alkanes.[37] Long-chain *n*-alcohols also display two *y*-phases, where the hydrocarbon chains are inclined by around 60^o to the plane of the unit cell.[35] At atmospheric pressure, the *y*-phases are generally preferred to the β-phase for long-chain *n*-alcohols (≥ C_{18}) containing an even number of carbon atoms, and very long *n*-alcohols (≥ C_{33}) with an odd number of carbon atoms.[35] For some other alcohols, such as isopropyl alcohol,[38] different polymorphs are known to dominate at high pressure (and ambient temperature) than at low temperature (and ambient pressure). Moreover, different rates of cooling or compression can favour different polymorphs.[39] Currently, it is not clear how pressure influences the solid-phase polymorphs formed by 1-dodecanol under EHL conditions.

In contrast to the fluid film thickness, EHL friction depends on the rheological properties of the lubricant film within the contact region, where pressures can exceed 1 GPa.[4] Matsuo and Makita[40] determined the viscosity of 1-dodecanol at temperatures between 25-75 °C and pressures up to 200 MPa. Bair[41] attempted to quantify the viscosity of 1-dodecanol at higher pressures. He found that at 40 °C, the viscosity of 1-dodecanol increased from 11 mPa·s at 0.1 MPa to 49 mPa·s at 5 MPa, but it quickly solidified before the pressure reached 100 MPa.[41] More recently, Carareto et al.[42] determined the high-pressure solid-liquid phase diagram of 1-dodecanol using microdifferential dcanning calorimetry (μDSC). They found that the solidification pressure of 1-dodecanol was around 80 MPa at 40 °C.[42]

Previous studies of 1-dodecanol EHL friction have suggested that very low friction could be achieved at high SRR in a steel-glass contact (maximum Hertz pressure = 0.57 GPa).[29] From the work of Bair[41] and Carareto et al.[42], it is expected that 1-dodecanol will solidify under these conditions. However, it is not clear whether low friction occurs for 1-dodecanol under other conditions relevant to EHL contacts. Moreover, the phyisicochemical changes leading to low friction in *n*-alcohols remain unclear.

In this study, we use EHL friction and film thickness measurements, Fourier transform infrared (FTIR) spectroscopy and polarised-light microscopy inside a diamond anvil cell (DAC), as well as differential scanning calorimetry (DSC), to explore the origins of the dimple formation and superlubricity of 1-dodecanol in EHL contacts. We show that the anomalous EHL film-formation and friction behaviour are due to polymorphic transformations. We uncover a novel superlubricity mechanism for 1-dodecanol, based on the formation of a lamellar hexagonal polymorph inside the contact.

2. METHODOLOGY

Materials

1-dodecanol (> 98 %) was purchased from Sigma Aldrich, UK (CAS number: 112-53-8) and used without further purification. It is the longest *n*-alcohol that is liquid at room temperature. This *n*-alcohol is low-cost and can be sourced from renewable resources.[43] AISI 52100 steel and glass balls and disks for the tribometer tests were purchased from PCS Instruments, UK.

EHL Friction

Friction coefficients in the full-film EHL regime were determined using a mini-traction machine (MTM) from PCS Instruments, UK. The MTM is shown schematically in Figure 2a.

In the MTM, a ball and disc are loaded together and independently driven to allow any combination of entrainment speed and sliding speed (and thus SRR).[44] The resulting friction force is measured by a piezoelectric transducer connected to the ball shaft. Three different surface combinations: steel-steel, steel-glass, and glass-glass, were used to obtain different contact pressures. Through-hardened AISI 52100 steel has an elastic modulus, E = 207 GPa and a Poisson's ratio, υ = 0.3,[45] while for glass E = 81 GPa and υ = 0.208.[20] The balls had a diameter of 19.05 mm. The contact was submerged in a temperature-controlled lubricant bath (accurate to ± 1 °C) to ensure that a fluid film was entrained into the contact.

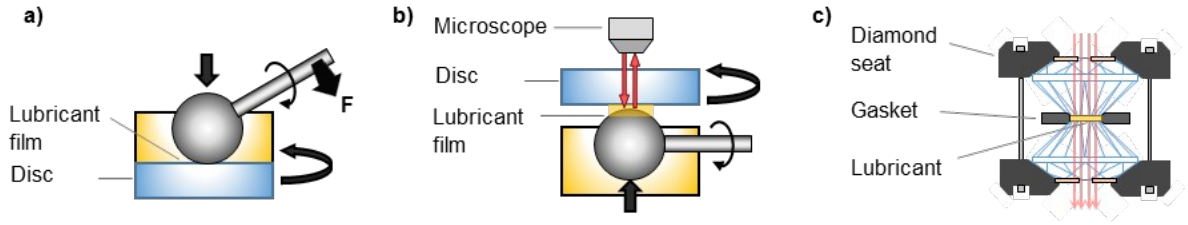

Figure 2. Schematic diagrams of test apparatus, (a) MTM to measure EHL friction, (b) EHD2 rig to measure EHL film thickness, and (c) DAC for high-pressure microscopy and spectroscopy.

The load was varied between 1-50 N, yielding mean Hertz pressures of between 0.1-1.1 GPa in the steel-glass contacts. This pressure range is representative of the conditions inside gears, bearings, constant velocity joints, and cam/ follower systems.[4] Most of the friction tests were run at 40 °C, although a subset of tests were run at higher temperatures (50-100 °C). The studied temperature range is representative of the operating conditions of lubricated components in ICE-powered vehicles.[5] The entrainment speed (2 m s^{-1}) and sliding speed (1 m s^{-1}) were both held constant, meaning that the SRR = 50 %. A subset of tests was also performed at higher SRR. No measurable wear occurred in any of the tribometer tests.

The frictional temperature rise in the contact is calculated to be from 0.7 °C (steel-steel)[24] to 3.2 °C (glass-glass)[46] for test conditions that are expected to generate the most heat (50 N load, steel-steel contact, 1 m s^{-1} sliding speed).[47] This temperature rise is sufficiently low to suggest that frictional heating does not play a significant role in the observed mechanisms.

EHL film thickness

EHL film thickness was measured using an EHD2 rig (PCS Instruments). This comprises a glass disc loaded against a 19.05 mm diameter AISI 52100 steel ball, the latter being partially submerged in lubricant, which is entrained between the specimens during rotation (Figure 2b). The disc is coated with a chromium and a silica layer with thicknesses of approximately 20 and 500 nm respectively, which enables central film thickness to be obtained by ultrathin-film interferometry.[48] This technique was used to obtain the EHL film thickness maps shown in Figure 1. Film thickness maps of the contact were also acquired using spacer layer image mapping (SLIM). In this technique, the reflected light is captured by an RGB CCD camera and film thickness values are obtained by comparing pixel intensity values to calibration data obtained under known conditions.[49]

Another purpose of the EHL film thickness tests was to confirm that the MTM friction measurements were obtained under full-film conditions. This is usually assessed using the ratio of the composite root-mean-square (RMS) surface roughness to fluid film thickness, which is known as the λ ratio. When $\lambda > 5$, friction experiments are generally assumed to be in the full-film EHL regime,[50] where friction is not affected by surface rougness.[51] In our MTM tests, the composite RMS surface roughness is 7 nm for the glass-glass contact, 11 nm for the glass-steel, and 13 nm for the steel-steel. For the steel-steel tests at the highest load (50 N) and 40 °C, the fluid film thickness is approximately 113 nm. Thus, the λ ratio is ~9 for the majority of the friction measurements presented in this study. Full details of these calculations is given in the Supporting Information. For the same contact at 50 N and 100 °C, the film thickness dropped to 31 nm and the λ ratio to 2.4. Thus, for the conditions leading to the thinnest fluid film, asperity contact may have resulted in a slight increase in friction.

DAC FTIR

FTIR spectroscopy of 1-dodecanol at high pressures inside a DAC was carried out at the Multimode InfraRed Imaging and Microspectroscopy (MIRIAM) beamline (B22) at Diamond Light Source.[52] A schematic of the DAC is shown in Figure 2c. A sample of 1-dodecanol was loaded into a mechanical DAC containing Type II diamond anvils with 400 μm culets (Almax, USA) and a stainless-steel gasket preindented to 35 μm thickness with a 300 μm diameter hole.[53] A ruby sphere (~20 μm diameter) was loaded for fluorescence pressure measurements.[54] The sample was taken to a pressure of 1.5 GPa, as determined using a Bruker Senterra Raman microscope with a HeNe laser source at 632.8 nm. After depressurization, ambient measurements were taken using the thin-film residue on one of the anvils for comparison to previous literature. FTIR spectra were collected with a Bruker

Vertex 80V FTIR spectrometer equipped with a KBr beam-splitter coupled to a Hyperion 3000 microscope equipped with a 50 µm sized liquid nitrogen cooled mercury cadmium telluride (MCT) detector. Spectra were collected at a resolution of 4 cm^{-1} and the number of co-added scans was 256.

DAC polarised-light microscopy

A Leica petrographic microscope was used to study the habits of the crystals formed by 1-dodecanol under pressure inside a DAC.[55] The hole was drilled (with a 400 µm tungsten bit) approximately normal to the gasket surface. Images were taken at room temperature (25 °C) and pressures between 0.15 GPa and 1.5 GPa. The combination of a large diamond culet (800 µm) and gasket hole diameter (400 µm) facilitates fine-tuning and an even application of pressure, which is essential for the relatively low pressures studied here. Both plane-polarised and cross-polarised polychromatic (white) light were used in transmission mode. The use of cross-polarised light registers birefringence from crystals and thereby allows much more textural detail to be seen than is the case for uncrossed polarisers.

DSC

DSC was used to detect phase transformations in 1-dodecanol by measuring the amount of heat required to increase or decrease the temperature of the sample at a constant rate.[36,56] Endothermic or exothermic phase transformations were detected by changes in heat input as energy is absorbed or emitted. The 1-dodecanol sample temperature was decreased from 60 to -20 °C and back again, with heating and cooling rates between 10-40 °C min^{-1}. All of the DSC experiments were performed at ambient pressure (0.1 MPa). These cooling rates are much higher than the µDSC experiments by Carareto et al.[42] (0.01 °C min^{-1}). DSC scans were also performed for shorter (1-decanol) and longer (1-tertradecanol and 1-hexadecanol) *n*-alcohols.

3. RESULTS

First, we test the hypothesis that 1-dodecanol undergoes pressure-induced solidification and polymorphic transformations inside EHL contacts. Then, we use *in-situ* and *ex-situ* analysis to investigate the links between these phase transformations and the dimple formation[21] and superlubricity[29] for 1-dodecanol. Figure 3a shows schematically the Hertz pressure distribution in an EHL contact. The mean pressure is approximately 66 % of the maximum pressure.

Tribometer Experiments

Figure 3b shows the results from an MTM, ball-on-disc friction test in which a constant SRR (50 %) and temperature (40 °C) are maintained, while the load is varied between 1-50 N. Three plots are shown, which result from three contact configurations: steel-steel, steel-glass, and glass-glass. Throughout these tests, the entrainment of lubricant was sufficient to hydrodynamically separate the surfaces, such that the measured friction arose from fluid shear only (negligible asperity contact).[51] Instead of a continuous increase in friction with load as is expected for most known lubricants, there is a low-load region where the friction is very low and nearly constant with load. At higher load, a discontinuity appears followed by a high-load region where friction increases and asymptotically approaches a constant value. A key observation from Figure 3b is that, for all three contacts, although they contain different material combinations, they show the abrupt friction increase at the same contact pressure (~0.5 GPa). This suggests that the discontinuity in each graph occurs when the maximum pressure in the contact reaches a phase-change pressure of 1-dodecanol. Bair[41] has shown previously that 1-dodecanol undergoes pressure-induced solidification at much lower pressures than the friction transition pressure (< 100 MPa) at 40 °C. Moreover, solid-liquid equilibria of 1-dodecanol using μDSC by Carareto et al.[42] suggested that the freezing pressure at 40 °C is expected to be around 80 MPa. Therefore, we suggest that the friction transition at around 0.5 GPa is due to a pressure-induced polymorphic transformation in 1-dodecanol.[34] Below the transition pressure, a low-friction polymorph is formed, while above this pressure, a high-friction polymorph is formed. Previous studies have confirmed that alcohols can form different polymorphs at high pressure than they do at low temperature.[38] In 1-hexanol, three phase transformations are observed during compression; the liquid solidifies to form a *γ*-phase at 0.8 GPa, which transforms into a *β*-phase at around 3.0 GPa, and another *β*-phase at around 7.3 GPa.[57] Longer *n*-alcohols, such as 1-tetradecanol and 1-octadecanol, are known to form *α*-phases as well as *β*-phases and *γ*-phases at atmospheric pressure.[36] However, high-pressure polymorphism has not been studied in these longer-chain *n*-alcohols.

In the SLIM images in Figure 3c, the size of the light green region, which indicates an increase in central film thickness, grows as the load is increased. This indicates that the size of the high-friction phase increases to cover a larger proportion of the contact above pressures of 0.5 GPa. This transition pressure also corresponds to the onset of dimple formation observed by Wang and Reddyhoff[21] (Figure 1).

It is possible to predict the average friction coefficient in the contact using simple Hertz analysis as detailed below. This is based on the approximation that the friction coefficient of 1-dodecanol has a constant value, μ_L, at pressures below the critical pressure, p_H, and a

constant value, μ_H, above p_H (Figure 3a). These coefficients are then weighted according to the fraction of the total load, W, supported by each region, found by integrating the two regions of the Hertz pressure distribution. Thus, the total friction coefficient,

$$\mu = \mu_L + \left\langle 1 - p_H^3 \times \left[\frac{\pi^3 R^2}{6 W E'^2} \right] \right\rangle (\mu_H - \mu_L) \quad (1)$$

where R and E' are the reduced radius and elastic modulus of the surfaces, respectively. Figure 3b shows that there is good agreement between the experimental friction coefficient vs. load results and Equation 1, with the only adjustable constants being p_H = 0.5 GPa, μ_L = 0.0005, and μ_H = 0.04 (the same values were used for all three fits). This suggests that a phase change is occurring within the contact at a specific pressure, irrespective of the contact stiffness and surface chemistry associated with the different specimen combinations. This is further confirmed when friction coefficients for the different material combinations are plotted against contact pressure and all collapse onto a single curve, as shown in the Supporting Information.

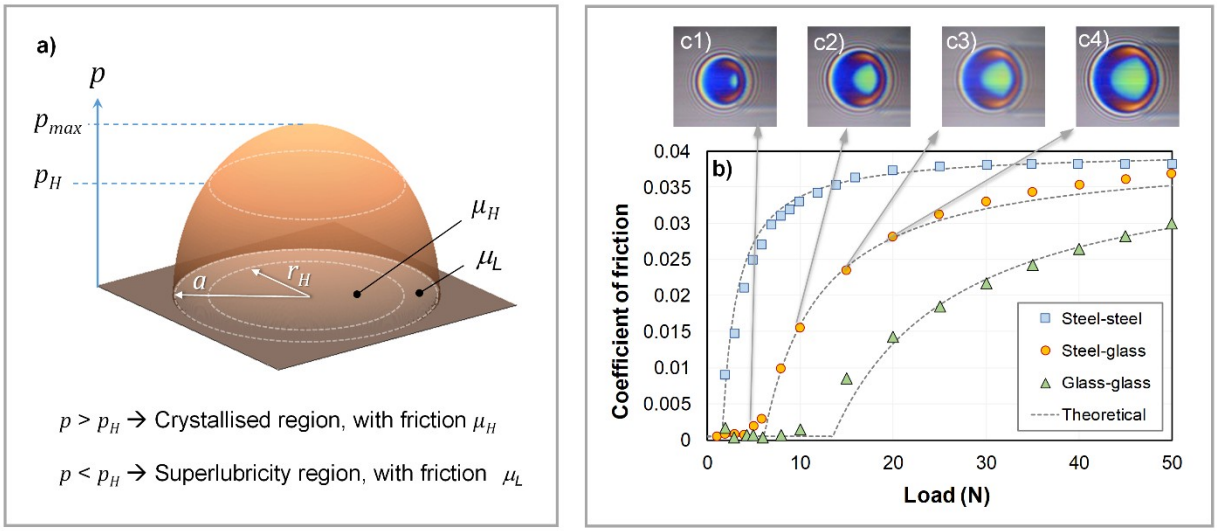

Figure 3. (a) Representation of contact pressure and friction coefficient distribution for phase-changing lubricant, (b) Friction coefficient vs. load for 1-dodecanol lubricated contact, with 2 m s^{-1} entrainment speed, 1 m s^{-1} sliding speed (SRR = 50 %) and 40°C inlet temperature, (c) SLIM images from steel-glass contact under the same conditions (central dimple region shown by light green colour).

An important feature in Figure 3b is the extremely low EHL friction coefficient of ~0.0005, which occurs below the polymorphic transformation pressure, p_H. Such low values of the friction coefficient are subject to large uncertainties.[58] However, the friction coefficient is

certainly sufficiently low (μ < 0.01) to be considered as an example of liquid superlubricity[8] and is two orders of magnitude lower than EHL friction measurements for conventional lubricants.[7] Thus, below the phase change pressure, 1-dodecanol could be expected to reduce total fuel consumption by ICE-powered vehicles by around 6 %.[5] Tribometer experiments similar to those shown in Figure 3b were also performed for a range of SRRs (see Supporting Information). These show that the observed phase transformations and the resultant friction behaviour are largely independent of the applied shear rate.

In the SLIM images from the glass-steel contact in Figure 3c, the colour of the contact inlet remains the same shade of dark blue (*i.e.* the film thickness is approximately constant) irrespective of the applied load. This shows that the flow of lubricant into the contact is unaffected by the phase transformation, since this only occurs in the centre of the contact, where the pressure is sufficiently high.

Following the hypothesis that a polymorphic transformation occurs when 1-dodecanol reaches a pressure of 0.5 GPa at 40 °C, low-high friction transitions would also be expected to occur at other pressure-temperature conditions. To test this, friction coefficient *vs.* load tests were conducted at a range of other temperatures (40-80 °C). The results for some representative temperatures for steel-glass contacts are shown in Figure 4a. The transition pressure (white-fill data points in Figure 4a) corresponds to the pressure at which there is the maximum increase in gradient of the friction coefficient with pressure. As expected, the transition pressure in Figure 4a increases with increasing temperature.

Figure 4b shows the low-high friction transition pressure at different pressure-temperature conditions, as well as solid-liquid phase equilibria data from Carareto et al.[42] measured up to 80 MPa. The liquidus obtained by Carareto et al.[42] is linearly extrapolated to higher pressures, which is a reasonable approximation since it has been shown to remain linear up to GPa-level pressures for *n*-alkanes of similar chain-length.[59] From Figure 4b, it is clear that 1-dodecanol will solidify in the central region of the contact under all of the conditions studied in the tribometer tests. This confirms that the low-high friction transition is due to high-pressure polymorphic phase transformations,[34] rather than a liquid-solid transition. Also marked on Figure 4b is the region of anomalously low friction that occurs at pressures just below, and temperatures just above the friction transition points. Both the solidification and polymorphic transformation pressures increase linearly with increasing temperature, the former with a shallower gradient than the latter. Such behaviour is not uncommon in high-pressure polymorphic phase diagrams.[60] For large systems (*e.g.* polymers and colloids), the application of shear can affect the temperature and pressure conditions under which liquid-

solid phase transitions occur.[61] However, shear is not expected to significantly shift the position of the liquid-solid transition for the relatively small *n*-dodecanol molecules studied here. Nonequilibrium molecular dynamics (NEMD) simulations have shown that while the crystallisation of *n*-hexacontane is significantly enhanced by shear, it has a much weaker effect for shorter-chain *n*-eicosane.[62] Another potential effect of shear is to promote melting at high shear rates through frictional heating. Since frictional heating is always < 4 °C under the conditions studied here (Supporting Information),[24] shear-induced melting is also not expected to play a major role in the phase transformations.

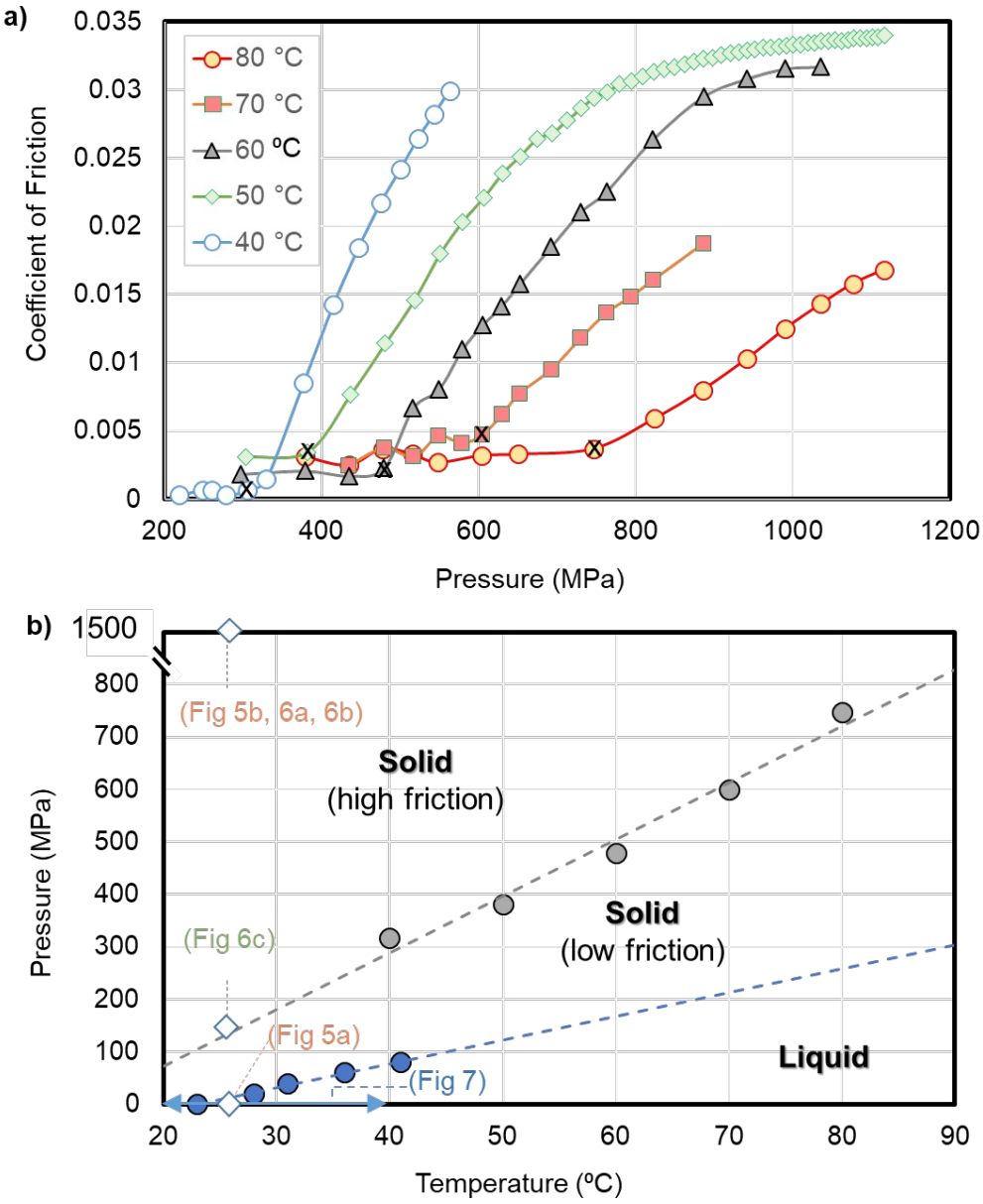

Figure 4. (a) Change in 1-dodecanol friction coefficient with maximum Hertz pressure for glass-steel (40 °C) and steel-steel (50-80 °C) contacts. Load and temperature varied using

an MTM with an entrainment speed of 2 m s^{-1} and a sliding speed of 1 m s^{-1} (SRR = 50 %). Points filled with a cross indicate the polymorphic ($\alpha \rightarrow \beta$) transformation pressure. (b) Solid-liquid phase diagram (blue circles) and transition between low and high friction phases (gray circles). Solid-liquid equilibria data from μDSC by Carareto et al.[42] and MTM friction data from (a). Dashed lines are linear fits to the data. Open diamonds show conditions for DAC and DSC experiments (Figures 5-7).

DAC Experiments

Ex-situ analysis was used to gain insights into the phase change behaviour of 1-dodecanol, comparing different points on the phase diagram (Figure 4b). First, a DAC was used to obtain FTIR spectra of 1-dodecanol at 25 °C and atmospheric (0.1 MPa) or high (1.5 GPa) pressure, as shown in Figure 5. These measurements were collected at B22, Diamond Light Source.[52] Vibrational assignments have been made based on Socrates.[63] The atmospheric pressure spectrum is consistent with previous literature for liquid-phase 1-dodecanol.[64] In the 1.5 GPa spectrum, the CH_2 and CH_3 peaks at 1000 cm^{-1} and 1400 cm^{-1} have intensified, and the OH peak at ~3200 cm^{-1} has shifted and intensified compared to their ambient condition positions. The intensification of CH_2 and CH_3 peaks is associated with pressure-induced solidification.[65] The behaviour of the OH peak suggests the formation of a network of hydrogen-bonded hydroxyl groups, which has previously been associated with solidification by cooling in *n*-octanol[66] and by pressurization in formic acid.[65] Simultaneous visual observations in the DAC confirmed this phase change, which was reversible on depressurization. This observation is supported by Figure 3c, which shows that the thick-film region ends before the lubricant exits the contact. This is where the pressure falls below the solid-liquid transition point.

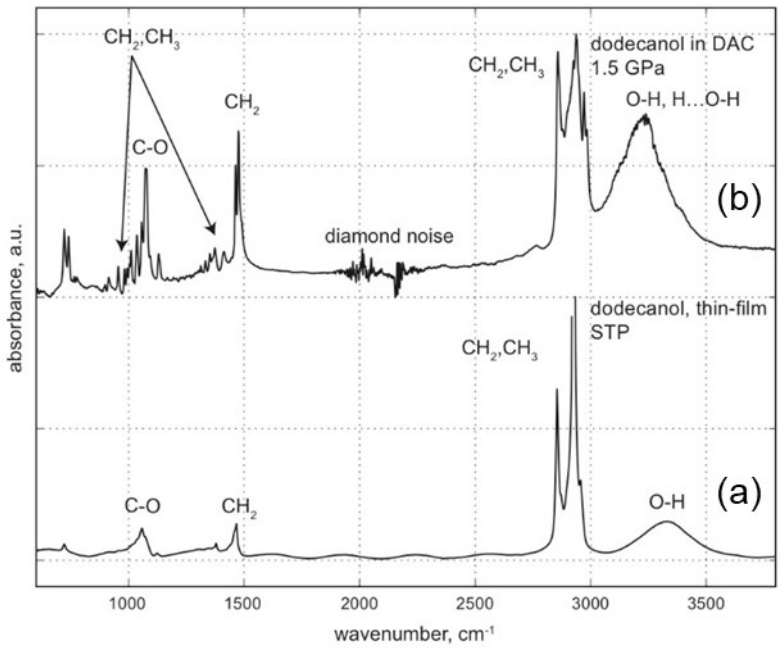

Figure 5. FTIR spectra from diamond anvil cell at 25 °C and 0.1 MPa (a) and 25 °C and 1.5 GPa (b). Vibrational assignments have been made based on Socrates.[63] Measurements made at B22, Diamond Light Source.[52]

A separate DAC was then used to obtain polarised-light microscopy images at 25 °C and 0.15 GPa and 25 °C and 1.5 GPa, using plane-polarised and cross-polarised light. The DAC was initially pressurised to 1.5 GPa to ensure sealing. Figure 6a, which was obtained using plane-polarised light, shows a mass of randomly-oriented interlocking fine-grained, needle-like crystals. The crystals are typically < 1 µm wide and up to 200 µm long. Diamond-shaped crystals have previously been obtained for orthorhombic *n*-alkanes of similar chain-length slowly cooled below their melting point.[67] Acicular crystals are usually formed when layer-by-layer growth is sufficiently slow such that there is competition with surface-activated secondary nucleation.[68] Needle-like textures are also characteristic of rapid crystallisation,[69] encouraged by the short duration (< 2 s) over which the pressure was increased from 0.1 MPa to 1.5 GPa in the DAC. This rapid application of pressure is consistent with that experienced by the 1-dodecanol molecules entrained in the tribometer experiments under EHL conditions. The rate of cooling or compression is an important variable since in many cases high-pressure polymorphic transformations are governed more by kinetic than thermodynamic factors.[39,70] Close examination of crystals in cross-polarised light (Figure 6b) reveals that they show optical extinction for both parallel and perpendicular to polarisers, a feature consistent with orthorhombic symmetry.[71] The birefringence seen in Figure 6b clarifies the texture and random orientation of the acicular crystals.

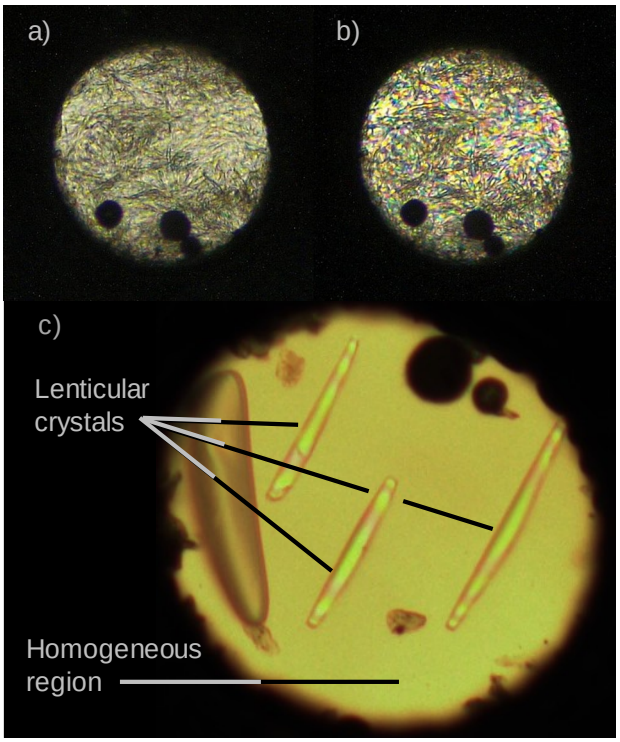

Figure 6. Polarised-light microscopy images of DAC chamber with 1-dodecanol at 25 °C and 1.5 GPa (a) and (b), 25 °C and ~0.15 GPa (c). The field of view is 400 µm. Image (a) was obtained using plane-polarized white light in transmission. Images (b) and (c) were obtained using cross-polarized white light in transmission.

The DAC was then carefully depressurised by hand to ~0.15 GPa at 25 °C, corresponding to conditions within the low-friction region in the tribometer experiments (see Figure 4b). Figure 6c shows a homogeneous region in which three curved, elongated crystals have formed. each showing a habit that is consistent with a hexagonal (rotator) phase.[67] These crystals grow from 1-dodecanol within seconds, initially appearing as small oriented blebs (< 50 µm long) with curved edges and terminations. These blebs coarsen rapidly and lengthen into the crystals shown in Figure 6c, which are 150-200 µm long and ~10 µm wide. The lenticular crystals in Figure 6c show slight bulging in the middle section of each crystal. Parallel orientation of the crystals (and their original blebs) is evident and is defined by their long axes being perpendicular to the major axis of the slightly elliptical chamber. Note that sample chamber ellipticity is a common feature of DACs with large drilled holes. This stress-orientation of the crystals[72] is not apparent at higher pressure (Figure 6a-b) where the crystals are randomly orientated. The parallel orientation of the crystals suggests that the 1-dodecanol liquid phase transmits stress non-hydrostatically during crystal formation.[72] The most likely cause for this observation is structural anisotropy, perhaps be due to the lamellar self-assembly of hydrogen-bonded chain-like clusters, which are known to form for long-

chain *n*-alcohols in the liquid phase.[31] The formation of stress-oriented lenticular crystals parallel to the sliding surfaces could be another contributing physical mechanism causing the very low EHL friction in the tribometer experiments.

DSC Experiments

DSC was used to study the phase changes occurring upon heating and cooling at atmospheric pressure. The results are shown in Figure 7. During cooling, two endotherms are observed that, according to Zuo et al.[56] and Carreto et al.[36], correspond to phase changes, from liquid to hexagonal crystal (*α*-phase) to orthorhombic crystal (*β*-phase). Schematics of the molecular packing in the *α*-phase and *β*-phase are shown in Figure 7a. The temperature at which hexagonal crystals form is independent of cooling rate in the range studied. Conversely, the temperature at which orthorhombic crystallisation occurs decreases with increasing cooling rate. The maximum achievable DSC cooling rate of 40 °C min^{-1} is low compared to the rate of pressure increase that 1-dodecanol experiences inside an EHL contact. For the data presented in Figure 3 and Figure 4, the pressure of the lubricant flowing through the contact will increase from 0.1 MPa to 0.5 GPa in ~50 µs. Therefore, it seems likely that the formation of orthorhombic crystals will be inhibited in EHL contacts. At moderate pressure (< 0.5 GPa), 1-dodecanol remains kinetically trapped in the less thermodynamically favourable *α*-phase.[70] At higher pressures, transformation from the low-density *α*-phase to the more stable *β*-phase,[35] eventually becomes inevitable.

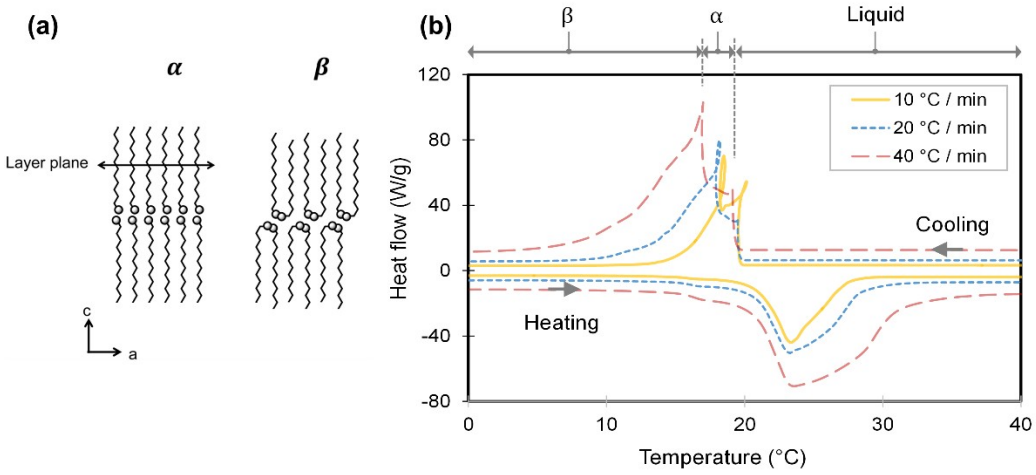

Figure 7. (a) Schematic showing molecular packing of *α*-phase and *β*-phase of 1-dodecanol (adapted from Zhu and Dhinojwala[73]), (b) DSC scans for 1-dodecanol at different cooling rates (10-40 °C min^{-1}). Phases marked at the top correspond to rapid cooling (40 °C min^{-1}).

At an intermediate cooling rate (20 °C min^{-1}), longer *n*-alcohols (1-tetradecanol, 1-hexadecanol, and 1-octadecanol) show more pronounced peaks for the hexagonal *α*-phase compared to the orthorhombic *β*-phase (Supporting Information). This implies that the low-friction *α*-phase is more stable for these molecules, meaning that it could potentially be sustained under higher pressures. Unlike 1-dodecanol, however, these *n*-alcohols are not liquids at room temperature.

4. DISCUSSION

Our results (Figure 4) demonstrate that 1-dodecanol crystallises due to pressure-induced hydrogen bonding when it is entrained into EHL contacts. This implies that the molecules are sufficiently distorted to overcome steric hindrances so that hydroxyl groups are brought to within 2.8 Å of each other, as is required to form a fully hydrogen-bonded aggregate.[74] An increase in hydrogen bonding at high pressure was confirmed by the FTIR spectra inside the DAC (Figure 5). The proposed behaviour for 1-dodecanol is consistent with previous investigations of shorter chain alcohols, such as methanol,[75] ethanol,[76] and phenol,[77] which have room temperature crystallisation pressures of 3.5 GPa,[75] 1.9 GPa,[76] and 0.16 GPa,[77] respectively. When conventional lubricants undergo pressure-induced solidification inside tribological contacts, they generally form an amorphous glassy phase that shows high EHL friction.[78] Some exceptions exist, for example *n*-dodecane monolayers showed microscale superlubricity when confined between atomically-smooth mica surfaces.[15]

In the current study, two different 1-dodecanol polymorphs were formed depending on the temperature and maximum Hertz pressure. At moderate temperature (40 °C) and pressure (≤ 0.5 GPa), a low-friction polymorph (Figure 3) is formed, which our *ex-situ* analysis (Figure 6-7) suggest is a hexagonal *α*-phase. At higher pressure, 1-dodecanol undergoes a polymorphic transformation to a high-friction (Figure 3) orthorhombic crystal (Figure 6-7). The polymorphic transformation pressure increases linearly with pressure with a gradient that is steeper than the liquidus (Figure 4). As the pressure increases above the hexagonal-orthorhombic transition, the friction coefficient increases, since the orthorhombic region grows to cover a greater proportion of the contact (Figure 3c). This increase in friction is accompanied by the formation of a dimple with locally increased film thickness (Figure 1c-d). Our results suggest that dimple formation[21,23] is driven by a bulging mechanism. In particular, 1-dodecanol enters the contact with an inclined (predominantly Couette) velocity profile due to the difference in speeds between the two bounding surfaces. As molecules approach the point in the contact where the pressure reaches the hexagonal-orthorhombic transformation pressure, the lubricant becomes increasingly rigid and the velocity gradient across the

thickness of the film approaches zero.[20] The uniform velocity beyond this point must be equal to the minimum of the entrained velocity profile (velocity of the slower surface), since anything faster than this would put the crystallised liquid under tension. This reduces the average velocity and in order to conserve the mass flow rate through the contact, the surfaces are pushed further apart, increasing the central film thickness. Towards the exit of the contact, the pressure first decreases to a level where first a orthorhombic-hexagonal transformation occurs, followed by melting. 1-dodecanol passing beyond this point can be easily sheared and so a Couette flow profile is recovered with an average velocity (and hence film thickness) equal to that of the pre-dimple inlet region (Figure 1).

Combined shear stress and hydrostatic pressure can induce polymorphic transformations in some materials.[79] For *n*-alkanes (C_{21}-C_{27}), it has been suggested that the favoured polymorph is shear rate (as well as pressure) dependant, with higher shear rates favouring the hexagonal (rotator) phase over the orthorhombic phase.[80] However, very high shear rates (300 s^{-1}) were applied in this previous study[80] and so the observed differences may in fact due to frictional heating within the contact.[24] Yagi et al.[29] showed that the friction of 1-dodecanol in glass-steel contacts increases to a maximum at low SSR, before decreasing with increasing SRR. Thus, in the tribometer experiments by Yagi et al.[29], there may have been a transformation from the high-friction to the low-friction polymorph at high SRR. Again, the possibility of the polymorphic transformation being driven by frictional heating,[24] rather than the shear stress, cannot be ruled out. We also tested the change in friction coefficient with SRR for 1-dodecanol in a steel-steel contact at different loads (see Supporting Information). In general, the friction coefficient increases sharply at low SRR and then remains approximately constant. This suggests that the polymorphic transformations are mostly pressure driven, rather than shear driven.

Below the hexagonal-orthorhombic transformation pressure, 1-dodecanol exhibits extremely low EHL friction ($\mu \approx 0.0005$), which can be classified as superlubricity (Figure 3).[8] The superlubricity mechanism for 1-dodecanol under EHL conditions is different to that observed for glycerol mono-oleate[18] and polyhydric alcohols[19] on DLC surfaces under boundary lubrication conditions. In these systems, mechanochemical decomposition of the molecules occurs, which passivates the sliding surfaces and promotes the formation of heterocyclic structures that facilitate superlow friction.[81] Friction coefficients close to the superlubricity threshold have been measured in previous EHL experiments for glycerol in steel-steel contacts.[82] This required the tribochemical decomposition of glycerol to water, which dramatically reduced the solution viscosity and thus EHL friction.[82]

The DAC (Figure 6) and DSC (Figure 7) results suggest that the anomalous low-friction region of the phase diagram coincides with the formation of a hydrogen bonded, hexagonal crystal. The resultant facile interlayer sliding between the lamellar hexagonal structures are believed to be responsible for the superlubricity of 1-dodecanol. Previous NEMD simulations showed that interlayer slip lead to very low friction in *n*-dodecane molecules confined between mica surfaces.[83] Interlayer sliding is responsible for the low friction achieved by many lubricant additives such as graphite,[84] graphene,[85] reduced graphene oxide,[86] and organomolybdenum compounds that form molybdenum disulphide.[87] Layered hexagonal structures are also responsible for structural superlubricity of two-dimensional materials such as graphite,[10] molybdenum disulphide,[11] graphene,[12] and graphene/boron nitride.[13] In these systems, lattice mismatches or heterojunctions between adjacent hexagonal layers eliminate the energy dissipation channels related to elastic instabilities and suppress stick-slip motion.[14] Thus, it is perhaps unsurprising that the hexagonal phase of 1-dodecanol gives much lower friction than the orthorhombic phase. This can be further rationalised from the observation that the hexagonal phase of *n*-alcohols is known to contain fewer gauche defects compared to the orthorhombic phase.[73] The reduction of gauche defects is known to reduce friction since it removes channels of energy dissipation during sliding.[88] In addition to molecular-scale factors, the formation of parallel lenticular crystals for the hexagonal phase, compared to randomly-orientated acicular crystals for the orthorhombic phase, could result in differences in friction at the microscale. It should be noted that this is not the first observation of dramatically variations in friction between different polymorphs. Paradinas et al.[89] showed that thiol self-assembled monolayers on gold surfaces can display both a low-friction rectangular *α*-phase and a high-friction oblique *β*-phase.

This discovery is distinct from other examples of liquid superlubricity in three key ways. Firstly, previous studies of liquid superlubricity involve permanent tribochemical transformations inside the contact,[17] whereas the superlubricious hexagonal arrangement of 1-dodecanol is temporarily induced by pressure-induced transformation, and subsequently returns to the liquid phase upon reaching the contact outlet (Figure 3c). Since the lubricant molecules are not consumed in the contact, the superlubricity is continuously self-replenishing. Secondly, most examples of superlubricity occur under boundary lubrication conditions for surface-confined layers, which are less than 10 nm in thickness.[14] In this study, superlubricity is achieved under full-film EHL conditions, with > 100 nm surface separations and > 100 μm contact diameters (Figure 1). Since the thickness of the 1-dodecanol bilayers (Figure 7) is approximately 3 nm, this implies that there are at least 30

bilayers separating the sliding surfaces, Thirdly, most other studies of superlubricity under liquid-lubricated conditions involve aqueous, rather than hydrocarbon-based lubricants. Superlubricity in these systems typically relies upon the very low pressure-viscosity coefficient of water,[90] which is not the case for 1-dodecanol.[41] The organic molecule used here is highly soluble in hydrocarbon lubricants and should be compatible with current lubrication systems. This combination of factors means that superlubricity can now be durable, self-replenishing, and compatible with hydrocarbon base oils. This enables its implementation in macroscale EHL contacts, such as bearings and gears. Durability of these components would also be improved since lower EHL friction can lead to longer fatigue life.[91]

The physical and chemical properties of neat *n*-alcohols (particularly low-temperature flow and oxidation stability[92]) differ from those stipulated in current lubricant specifications. Therefore, the challenge now is to facilitate this liquid superlubricity behaviour in a lubricant formulation that meets these specifications. This could be achieved either by blending a low concentration of *n*-alcohol with a base oil (*i.e.* using this self-assembly as an additive) or perhaps by adding alcohol groups to hydrocarbon base oil molecules. The former approach is likely to be successful since long-chain *n*-alcohols are highly soluble in hydrocarbons and previous studies have shown that more polar lubricant components aggregate near the sliding surfaces and dominate the overall tribological response.[93]

The results obtained in study suggest that *n*-alcohols could be an attractive option to lubricate bearings and gears in electric vehicles (EVs), since these will generally encounter lower pressures, but higher sliding speeds, compared to equivalent components in ICE-powered vechiles.[6] Thus, 1-dodecanol could provide superlubricity in more components in EVs than ICE-powered vehicles, under normal operating conditions. Another progression could be to test similar molecules to identify those that can maintain superlubricity at lower temperature and higher pressure.

5. CONCLUSIONS

In this study, we have shown that 1-dodecanol undergoes pressure-induced solidification due to enhanced hydrogen-bonding inside EHL contacts. The EHL friction and film-formation behaviour of 1-dodecanol are insensitive to the surface chemistry or roughness. Depending on the temperature and pressure conditions, two polymorphs with different friction coefficients can be formed. At high pressure and low temperature, an orthorhombic polymorph is formed that leads to anomalous dimple formation and relatively high friction. At

low pressure and high temperature, a hexagonal polymorph is formed that exhibits robust macroscale superlubricity. The lamellar structure of the hexagonal polymorph facilitates interlayer sliding, similar to two-dimensional materials used as solid lubricants. This system, however, maintains the many practical advantages of liquid lubricants. Superlubricity of 1-dodecanol is observed on both glass and steel surfaces, suggesting it is not sensitive to surface chemistry or topology. Moreover, 1-dodecanol returns to the liquid state upon leaving the contact, so the superlubricity is continuously self-replenishing. The macroscale superlubricity observed for 1-dodecanol is therefore distinct from other liquid lubricants, which rely on tribochemical transformations and specific surface chemistries.

The discovery of superlubricity of 1-dodecanol under EHL conditions suggests that durability and efficiency gains of more than an order of magnitude are possible in components containing rolling-sliding contacts, such as bearings and gears. Since current lubricant specifications do not allow for neat n-alcohols to be used as lubricants, future work will focus on using *n*-alcohols within lubricant blends and as additives while maintaining superlubricity.

ACKNOWLEDGEMENTS

We thank Diamond Light Source for access to the MIRIAM beamline, B22, (SM16420) that contributed to the results presented here.[52] J.P.E. thanks the Royal Academy of Engineering for a Research Fellowship.

NOTES

T.R. declares the following competing financial interest: A patent application partially based on this work has been filed (Patent Application Number: PCT/GB2019/051014).

SUPPORTING INFORMATION

The Supporting Information is available free of charge on the ACS Publications website at DOI: xxxxx.

(i) Estimation of frictional heating effects, (ii) film thickness measurements (Figure S1), (iii) dependence of the friction coefficient on the contact pressure (Figure S2), (iv) Hertz Analysis, (v) effect of shear rate on friction (Figure S3), and (vi) DSC data for n-alcohols with different chain lengths (Figure S4).

REFERENCES

(1) Holmberg, K.; Erdemir, A. Influence of Tribology on Global Energy Consumption, Costs and Emissions. *Friction* **2017**, *5*, 263–284.

(2) Gabelli, A.; Voskamp A P; Shearer, S.; Ionannides, E. The Service Life of Rolling Element Bearings - Stress Field and Material Response Analysis. *VDI Berichte* **1998**, *1380*, 171–195.

(3) Dowson, D.; Higginson, G. R. A Numerical Solution to the Elasto-Hydrodynamic Problem. *J. Mech. Eng. Sci.* **1959**, *1*, 6–15.

(4) Spikes, H.; Jie, Z. History, Origins and Prediction of Elastohydrodynamic Friction. *Tribol. Lett.* **2014**, *56*, 1–25.

(5) Holmberg, K.; Andersson, P.; Erdemir, A. Global Energy Consumption Due to Friction in Passenger Cars. *Tribol. Int.* **2012**, *47*, 221–234.

(6) Holmberg, K.; Erdemir, A. The Impact of Tribology on Energy Use and CO2 Emission Globally and in Combustion Engine and Electric Cars. *Tribol. Int.* **2019**, *135*, 389–396.

(7) Zhang, J.; Tan, A.; Spikes, H. Effect of Base Oil Structure on Elastohydrodynamic Friction. *Tribol. Lett.* **2017**, *65*, 13.

(8) Martin, J. M.; Erdemir, A. Superlubricity: Friction's Vanishing Act. *Phys. Today* **2018**, *71*, 40–45.

(9) Hirano, M.; Shinjo, K. Atomistic Locking and Friction. *Phys. Rev. B* **1990**, *41*, 11837–11851.

(10) Dienwiebel, M.; Verhoeven, G. S.; Pradeep, N.; Frenken, J. W. M.; Heimberg, J. A.; Zandbergen, H. W. Superlubricity of Graphite. *Phys. Rev. Lett.* **2004**, *92*, 126101.

(11) Martin, J. M.; Donnet, C.; Le Mogne, T.; Epicier, T. Superlubricity of Molybdenum Disulphide. *Phys. Rev. B* **1993**, *48*, 10583(R).

(12) Feng, X.; Kwon, S.; Park, J. Y.; Salmeron, M. Superlubric Sliding of Graphene Nanoflakes on Graphene. *ACS Nano* **2013**, *7*, 1718–1724.

(13) Mandelli, D.; Leven, I.; Hod, O.; Urbakh, M. Sliding Friction of Graphene/Hexagonal-Boron Nitride Heterojunctions: A Route to Robust Superlubricity. *Sci. Rep.* **2017**, *7*, 10851.

(14) Hod, O.; Meyer, E.; Zheng, Q.; Urbakh, M. Structural Superlubricity and Ultralow Friction across the Length Scales. *Nature* **2018**, *563*, 485–492.

(15) Smith, A. M.; Hallett, J. E.; Perkin, S. Solidification and Superlubricity with Molecular Alkane Films. *Proc. Natl. Acad. Sci. USA* **2019**, *116*, 25418–25423.

(16) Berman, D.; Deshmukh, S. A.; Sankaranarayanan, S. K. R. S.; Erdemir, A.; Sumant, A. V. Macroscale Superlubricity Enabled by Graphene Nanoscroll Formation. *Science.* **2015**, *348*, 1118–1122.

(17) Ge, X.; Li, J.; Luo, J. Macroscale Superlubricity Achieved With Various Liquid Molecules: A Review. *Front. Mech. Eng.* **2019**, *5*, 2.

(18) Kano, M.; Yasuda, Y.; Okamoto, Y.; Mabuchi, Y.; Hamada, T.; Ueno, T.; Ye, J.; Konishi, S.; Takeshima, S.; Martin, J. M.; De Barros Bouchet, M. I.; Le Mogne, T. Ultralow Friction of DLC in Presence of Glycerol Mono-Oleate (GMO). *Tribol. Lett.* **2005**, *18*, 245–251.

(19) Matta, C.; Joly-Pottuz, L.; De Barros Bouchet, M. I.; Martin, J. M.; Kano, M.; Zhang, Q.; Goddard III, W. A. Superlubricity and Tribochemistry of Polyhydric Alcohols. *Phys. Rev. B* **2008**, *78*, 085436.

(20) Ehret, P.; Dowson, D.; Taylor, C. M. On Lubricant Transport Conditions in Elastohydrodynamic Conjunctions. *Proc. R. Soc. London, Ser. A* **1998**, *454*, 763–787.

(21) Wang, P.; Reddyhoff, T. Wall Slip in an EHL Contact Lubricated with 1-Dodecanol. *Tribol. Int.* **2017**, *113*, 197–205.

(22) Foord, C. A.; Wedeven, L. D.; Westlake, F. J.; Cameron, A. Optical Elastohydrodynamics. *Proc. Inst. Mech. Eng.* **1969**, *184*, 487–505.

(23) Yagi, K.; Vergne, P. Abnormal Film Shapes in Sliding Elastohydrodynamic Contacts Lubricated by Fatty Alcohols. *Proc. Inst. Mech. Eng. Part J* **2007**, *221*, 287–300.

(24) Reddyhoff, T.; Schmidt, A.; Spikes, H. Thermal Conductivity and Flash Temperature. *Tribol. Lett.* **2019**, *67*, 22.

(25) Cameron, A. The Viscosity Wedge. *ASLE Trans.* **1958**, *1*, 248–253.

(26) Kaneta, M.; Nishikawa, H.; Kameishi, K.; Sakai, T.; Ohno, N. Effects of Elastic Moduli of Contact Surfaces in Elastohydrodynamic Lubrication. *J. Tribol.* **1992**, *114*, 75–80.

(27) Hamrock, B. J.; Dowson, D. Isothermal Elastohydrodynamic Lubrication of Point Contacts: Part III-Fully Flooded Results. *J. Lubr. Technol.* **1977**, *99*, 264–275.

(28) Yagi, K.; Sugimura, J.; Vergne, P. Rheological Response of Fatty Alcohols in Sliding Elastohydrodynamic Contacts. *Tribol. Int.* **2012**, *49*, 58–66.

(29) Yagi, K.; Nishida, K.; Sugimura, J. Relationship between the Molecular Structure of Lubricants and Appearance of Anomalous Film Shapes in Elastohydrodynamic Lubrication Conditions. *Tribol. Int.* **2020**, *152*, 106574.

(30) Sarkar, S.; Joarder, R. N. Molecular Clusters in Liquid Ethanol at Room Temperature. *J. Chem. Phys.* **1994**, *100*, 5118–5122.

(31) MacCallum, J. L.; Tieleman, D. P. Structures of Neat and Hydrated 1-Octanol from Computer Simulations. *J. Am. Chem. Soc.* **2002**, *124*, 15085–15093.

(32) Wallen, S. L.; Palmer, B. J.; Garrett, B. C.; Yonker, C. R. Density and Temperature Effects on the Hydrogen Bond Structure of Liquid Methanol. *J. Phys. Chem.* **1996**, *100*, 3959–3964.

(33) Fragiadakis, D.; Roland, C. M. Are Polar Liquids Less Simple? *J. Chem. Phys.* **2013**, *138*, 12A502.

(34) Ventolá, L.; Ramírez, M.; Calvet, T.; Solans, X.; Cuevas-Diarte, M. A.; Negrier, P.; Mondieig, D.; van Miltenburg, J. C.; Oonk, H. A. J. Polymorphism of N-Alkanols: 1-Heptadecanol, 1-Octadecanol, 1-Nonadecanol, and 1-Eicosanol. *Chem. Mater.* **2002**, *14*, 508–517.

(35) Tasumi, M.; Shimanouchi, T.; Watanabe, A.; Goto, R. Infrared Spectra of Normal Higher Alcohols-I. *Spectrochim. Acta* **1964**, *20*, 629–666.

(36) Carreto, L.; Almeida, A. R.; Fernandes, A. C.; Vaz, W. L. C. Thermotropic Mesomorphism of a Model System for the Plant Epicuticular Wax Layer. *Biophys. J.* **2002**, *82*, 530–540.

(37) Muller, A. X-Ray Investigation of Normal Paraffins. *Proc. R. Soc. London, Ser. A* **1932**, *138*, 514–530.

(38) Ridout, J.; Probert, M. R. Low-Temperature and High-Pressure Polymorphs of Isopropyl Alcohol. *CrystEngComm* **2014**, *16*, 7397–7400.

(39) Ridout, J.; Price, L. S.; Howard, J. A. K.; Probert, M. R. Polymorphism Arising from Differing Rates of Compression of Liquids. *Cryst. Growth Des.* **2014**, *14*, 3384–3391.

(40) Matsuo, S.; Makita, T. Viscosities of Six 1-Alkanols at Temperatures in the Range 298-348 K and Pressures up to 200 MPa. *Int. J. Thermophys.* **1989**, *10*, 833–843.

(41) Bair, S. Rheology and High-Pressure Models for Quantitative Elastohydrodynamics. *Proc. Inst. Mech. Eng. Part J* **2008**, *223*, 617–628.

(42) Carareto, N. D. D.; Costa, M. C.; Meirelles, A. J. A.; Pauly, J. High Pressure Solid-Liquid Equilibrium of Fatty Alcohols Binary Systems from 1-Dodecanol, 1-Tetradecanol, 1-Hexadecanol, and 1-Octadecanol. *J. Chem. Eng. Data* **2015**, *60*, 2966–2973.

(43) Thakur, D. S.; Kundu, A. Catalysts for Fatty Alcohol Production from Renewable Resources. *J. Am. Oil Chem. Soc.* **2016**, *93*, 1575–1593.

(44) LaFountain, A. R.; Johnston, G. J.; Spikes, H. A. The Elastohydrodynamic Traction of Synthetic Base Oil Blends. *Tribol. Trans.* **2001**, *44*, 648–656.

(45) Guo, Y. B.; Liu, C. R. Mechanical Properties of Hardened AISI 52100 Steel in Hard Machining Processes. *J. Manuf. Sci. Eng.* **2002**, *124*, 1–9.

(46) Kaneta, M.; Yang, P. Effects of Thermal Conductivity of Contacting Surfaces on Point EHL Contacts. *J. Tribol.* **2003**, *125*, 731–738.

(47) Kennedy, F. E. Thermal and Thermomechanical Effects in Dry Sliding. *Wear* **1984**, *100*, 453–476.

(48) Gohar, R.; Cameron, A. Optical Measurement of Film Thickness Under Elasto-Hydrodynamic Lubrication. *Nature* **1963**, *200*, 458–459.

(49) Cann, P. M.; Spikes, H. A.; Hutchinson, J. The Development of a Spacer Layer Imaging Method (SLIM) for Mapping Elastohydrodynamic Contacts. *Tribol. Trans.* **1996**, *39*, 915–921.

(50) Zhang, J.; Ewen, J. P.; Ueda, M.; Wong, J. S. S.; Spikes, H. A. Mechanochemistry of Zinc Dialkyldithiophosphate on Steel Surfaces under Elastohydrodynamic Lubrication Conditions. *ACS Appl. Mater. Interfaces* **2020**, *12*, 6662–6676.

(51) Evans, C. R.; Johnson, K. L. The Influence of Surface Roughness on

Elastohydrodynamic Traction. *Proc. Inst. Mech. Eng. Part C* **1987**, *201*, 145–150.

(52) Cinque, G.; Frogley, M.; Wehbe, K.; Filik, J.; Pijanka, J. Multimode Infrared Imaging and Microspectroscopy (MIRIAM) Beamline at Diamond. *Synchrotron Radiat. News* **2011**, *24*, 24–33.

(53) Chervin, J. C.; B. Canny; J. M. Besson; Ph. Pruzan. A Diamond Anvil Cell for IR Microspectroscopy. *Rev. Sci. Instrum.* **1995**, *66*, 2595.

(54) Mao, H. K.; Xu, J.; Bell, P. M. Calibration of the Ruby Pressure Gauge to 800 Kbar under Quasi-Hydrostatic Conditions. *J. Geophys. Res.* **1986**, *91*, 4673–4676.

(55) Takemura, K.; Shimomura, O.; Sawada, T. A Diamond Anvil Cell for Advanced Microscopic Observations and Its Application to the Study of Crystal Growth under Pressure. *Rev. Sci. Instrum.* **1989**, *60*, 3783–3788.

(56) Zuo, J.; Li, W.; Weng, L. Thermal Performance of Caprylic Acid/1-Dodecanol Eutectic Mixture as Phase Change Material (PCM). *Energy Build.* **2011**, *43*, 207–210.

(57) Ren, Y.; Cheng, X.; Zhu, X.; Yang, K.; Wang, Y.; Yuan, C. Raman and IR Studies of Polymorphism in N-Hexanol at High Pressure and Low Temperature. *J. Mol. Struct.* **2017**, *1144*, 9–13.

(58) Schmitz, T. L.; Action, J. E.; Ziegert, J. C.; Sawyer, W. G. The Difficulty of Measuring Low Friction: Uncertainty Analysis for Friction Coefficient Measurements. *J. Tribol.* **2005**, *127*, 673–678.

(59) Morawski, P.; Coutinho, J. A. P.; Domańska, U. High Pressure (Solid + Liquid) Equilibria of n-Alkane Mixtures: Experimental Results, Correlation and Prediction. *Fluid Phase Equilib.* **2005**, *230*, 72–80.

(60) Bridgman, P. W. Polymorphic Transitions of 35 Substances to 50,000 Kg/Cm2. *Proc. Am. Acad. Arts Sci.* **1937**, *72*, 45–136.

(61) Onuki, A. Phase Transitions of Fluids in Shear Flow. *J. Phys. Condens. Matter* **1997**, *6*, 6119.

(62) Jabbarzadeh, A.; Tanner, R. I. Crystallization of Alkanes under Quiescent and Shearing Conditions. *J. Nonnewton. Fluid Mech.* **2009**, *160*, 11–21.

(63) Socrates, G. *Infrared and Raman Characteristic Group Frequencies*, 3rd ed.; Wiley:

Chichester, 2001.

(64) Chen, Z. H.; Yu, F.; Zeng, X. R.; Zhang, Z. G. Preparation, Characterization and Thermal Properties of Nanocapsules Containing Phase Change Material n-Dodecanol by Miniemulsion Polymerization with Polymerizable Emulsifier. *Appl. Energy* **2012**, *91*, 7–12.

(65) Montgomery, W.; Zaug, J. M.; Howard, W. M.; Goncharov, A. F.; Crowhurst, J. C.; Jeanloz, R. Melting Curve and High-Pressure Chemistry of Formic Acid to 8 GPa and 600 K. *J. Phys. Chem. B* **2005**, *109*, 19443–19447.

(66) Vasileva, A.; Golub, P.; Doroshenko, I.; Pogorelov, V.; Sablinskas, V.; Balevicius, V.; Ceponkus, J. FTIR Spectra of N-Octanol in Liquid and Solid States. *Dataset Pap. Sci.* **2014**, 921308.

(67) Toda, A.; Miyaji, H.; Ogawa, Y.; Tanamizawa, K. Lateral Habits of N-Alkane Single Crystals. *J. Mater. Sci.* **1991**, *26*, 2793–2796.

(68) Puela, F.; Verduranda, E.; Taulelleb, P.; Bebona, C.; Colson, D.; Kleina, J.-P.; Veesler, S. Crystallization Mechanisms of Acicular Crystals. *J. Cryst. Growth* **2008**, *310*, 110–115.

(69) Gordon, J. E. Growth and the Breaking Strains of Certain Needle Crystals. *Nature* **1957**, *179*, 1270–1272.

(70) Boldyreva, E. High-Pressure Polymorphs of Molecular Solids: When Are They Formed, and When Are They Not? Some Examples of the Role of Kinetic Control. *Cryst. Growth Des.* **2007**, *7*, 1662–1668.

(71) Akizuki, M.; Harada, K. Symmetry, Twinning, and Parallel Growth of Scolecite, Mesolite, and Natrolite. *Am. Mineral.* **1988**, *73*, 613–618.

(72) Kamb, W. B. Theory of Preferred Crystal Orientation Developed by Crystallization under Stress. *J. Geol.* **1959**, *67*, 153–170.

(73) Zhu, H.; Dhinojwala, A. Thermal Behavior of Long-Chain Alcohols on Sapphire Substrate. *Langmuir* **2015**, *31*, 6306–6313.

(74) Brock, C. P.; Duncan, L. L. Anomalous Space-Group Frequencies for Monoalcohols CnHmOH. *Chem. Mater.* **1994**, *6*, 1307–1312.

(75) Allan, D. R.; Clark, S. J.; Brugmans, M. J. P.; Ackland, G. J.; Vos, W. L. Structure of Crystalline Methanol at High Pressure. *Phys. Rev. B* **1998**, *58*, R11809–R11812.

(76) Allan, D. R.; Clark, S. J. Comparison of the High-Pressure and Low-Temperature Structures of Ethanol and Acetic Acid. *Phys. Rev. B* **1999**, *60*, 6328–6334.

(77) Allan, D. R.; Clark, S. J.; Dawson, A.; McGregor, P. A.; Parsons, S. Pressure-Induced Polymorphism in Phenol. *Acta Crystallogr. Sect. B Struct. Sci.* **2002**, *58*, 1018–1024.

(78) Evans, C. R.; Johnson, K. L. The Rheological Properties of Elastohydrodynamic Lubricants. *Proc. Inst. Mech. Eng. Part C* **1986**, *200*, 303–312.

(79) Bridgman, P. W. Effects of High Shearing Stress Combined with High Hydrostatic Pressure. *Phys. Rev.* **1935**, *48*, 825–847.

(80) Sasaki, K.; Inayoshi, N.; Tashiro, K. In Situ FTIR-ATR Observation of Phase Transition Behavior of n-Alkane Molecules Induced by Friction Motion on a Metal Interface. *J. Phys. Chem. C* **2009**, *113*, 3287–3291.

(81) Kuwahara, T.; Romero, P. A.; Makowski, S.; Weihnacht, V.; Moras, G.; Moseler, M. Mechano-Chemical Decomposition of Organic Friction Modifiers with Multiple Reactive Centres Induces Superlubricity of Ta-C. *Nat. Commun.* **2019**, *10*, 151.

(82) Habchi, W.; Matta, C.; Joly-Pottuz, L.; De Barros, M. I.; Martin, J. M.; Vergne, P. Full Film, Boundary Lubrication and Tribochemistry in Steel Circular Contacts Lubricated with Glycerol. *Tribol. Lett.* **2011**, *42*, 351–358.

(83) Jabbarzadeh, A.; Harrowell, P.; Tanner, R. I. Very Low Friction State of a Dodecane Film Confined between Mica Surfaces. *Phys. Rev. Lett.* **2005**, *94*, 126103.

(84) Huang, H. D.; Tu, J. P.; Gan, L. P.; Li, C. Z. An Investigation on Tribological Properties of Graphite Nanosheets as Oil Additive. *Wear* **2006**, *261*, 140–144.

(85) Eswaraiah, V.; Sankaranarayanan, V.; Ramaprabhu, S. Graphene-Based Engine Oil Nanofluids for Tribological Applications. *ACS Appl. Mater. Interfaces* **2011**, *3*, 4221–4227.

(86) Mungse, H. P.; Khatri, O. P. Chemically Functionalized Reduced Graphene Oxide as a Novel Material for Reduction of Friction and Wear. *J. Phys. Chem. C* **2014**, *118*, 14394–14402.

(87) Topolovec Miklozic, K.; Graham, J.; Spikes, H. Chemical and Physical Analysis of Reaction Films Formed by Molybdenum Dialkyl-Dithiocarbamate Friction Modifier Additive Using Raman and Atomic Force Microscopy. *Tribol. Lett.* **2001**, *11*, 71–81.

(88) Mikulski, P. T.; Harrison, J. A. Packing-Density Effects on the Friction of n-Alkane Monolayers. *J. Am. Chem. Soc.* **2001**, *123*, 6873–6881.

(89) Paradinas, M.; Munuera, C.; Silien, C.; Buck, M.; Ocal, C. Heterogeneous Nanotribological Response of Polymorphic Self-Assembled Monolayers Arising from Domain and Phase Dependent Friction. *Phys. Chem. Chem. Phys.* **2013**, *15*, 1302–1309.

(90) Bridgman, P. W. The Viscosity of Liquids under Pressure. *Proc. Natl. Acad. Sci. U. S. A.* **1925**, *11*, 603–606.

(91) Rico, J. E. F.; Battez, A. H.; Cuervo, D. G. Rolling Contact Fatigue in Lubricated Contacts. *Tribol. Int.* **2003**, *36*, 35–40.

(92) Erhan, S. Z.; Sharma, B. K.; Perez, J. M. Oxidation and Low Temperature Stability of Vegetable Oil-Based Lubricants. *Ind. Crops Prod.* **2006**, *24*, 292–299.

(93) Gao, G.; Spikes, H. A. The Control of Friction by Molecular Fractionation of Base Fluid Mixtures at Metal Surfaces. *Tribol. Trans.* **1997**, *40*, 461–469.

GRAPHICAL ABSRACT

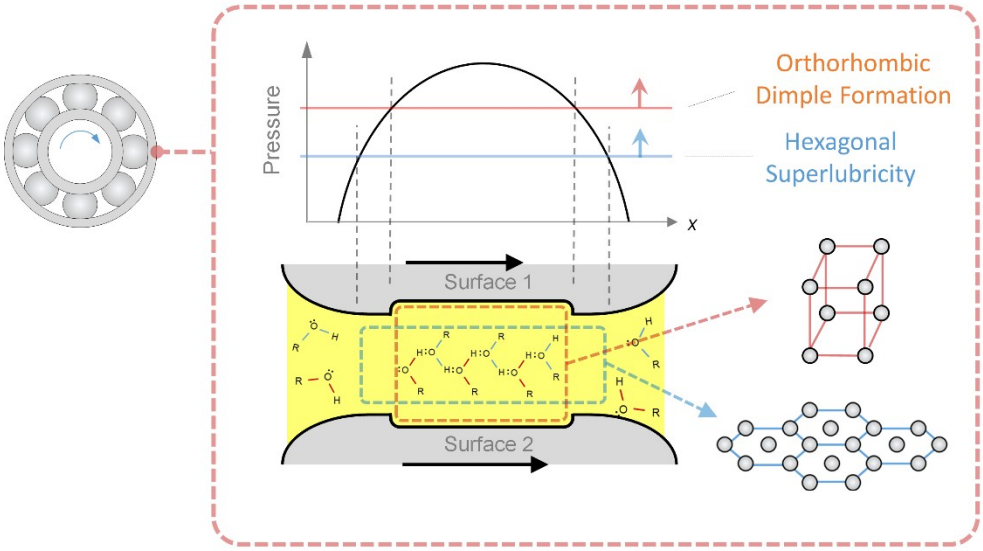
Pressure
x
Orthorhombic
Dimple Formation
Hexagonal
Superlubricity
Surface 1
Surface 2